DOI: 10.1002/chem.200600101

Unprecedented Association of $[Mo_6Br^i_7Y^iBr^a_6]^{3-}$ Cluster Units and $[Mo^{III}Br_6]^{3-}$ Complexes: Synthesis, Crystal Structures, and Properties of the Double Salts $Rb_3[Mo_6Br^i_7Y^iBr^a_6](Rb_3[MoBr_6])_3$ (Y = Se, Te)

Kaplan Kirakci, Stéphane Cordier,* and Christiane Perrin[a]

Abstract: The double salts $Rb_3[Mo_6Br^i_7Y^iBr^a_6](Rb_3[MoBr_6])_3$ (Y = Se, Te) result from the partial disproportionation of the Mo_6Br_{12} octahedral-cluster-based bromide, in the presence of corresponding chalcogenides and RbBr salt (crystal data: $Rb_{12}[MoBr_6]_3[Mo_6Br^i_7Te^iBr^a_6]$ (**1**), $Pm\bar{3}m$ (No. 221), $a = 12.1558(2)$ Å, $Z = 1$, $R_1 = 0.028$; $wR_2 = 0.050$; $Rb_{12}[MoBr_6]_3[Mo_6Br^i_7Se^iBr^a_6]$ (**2**), $Pm\bar{3}m$, $a = 12.144(3)$ Å, $Z = 1$, $R_1 = 0.028$; $wR_2 = 0.050$). The structures of **1** and **2** are built up from $[Mo^{III}Br_6]^{3-}$ complexes and $[Mo_6Br^i_7Y^iBr^a_6]^{3-}$ cluster units characterised by a random distribution of seven bromine and one chalcogen ligands on all the eight inner positions that face cap the Mo_6 clusters. Such a distribution implies a static orientational disorder of the $[Mo_6Br^i_7Y^iBr^a_6]^{3-}$ units around the origin of the unit cell. Close-packed anionic layers based on $[Mo^{III}Br_6]^{3-}$ complexes and $[Mo_6Br^i_7Y^iBr^a_6]^{3-}$ cluster units are stacked in the sequence ABC. This arrangement leads to very short Br^a–Br^a intercluster unit distances of 3.252 Å, much lower than the sum of the van der Waals radii (3.70 Å). The trivalent oxidation state of molybdenum in the Mo complexes and 24 valence electrons per Mo_6 cluster have been confirmed by magnetic susceptibility measurements. Salts **1** and **2** constitute the first examples of structurally characterised bromides containing discrete $[Mo^{III}Br_6]^{3-}$ complexes obtained by means of solid-state synthesis.

Keywords: anions · cluster compounds · halides · solid-state reactions · transition metals

Introduction

Structures of binary molybdenum halides with the general Mo_6X_{12} formula (X = Cl, Br, I) are based on octahedral Mo_6 clusters characterised by Mo–Mo bonds. Mo_6 metallic clusters were structurally characterised by Brosset,[1] but were first reported by Blomstrandt in 1857.[2] The Mo_6 clusters are bound to eight inner ligands located in face-capping positions (X^i) and to six apical ligands located in terminal positions (X^a) to form a $Mo_6X^i_8X^a_6$ anionic unit.[3] The structures of these Mo_6X_{12} halides are based on $Mo_6X^i_8X^a_6$ units that share four apical ligands with four adjacent units in the equatorial plane. These interconnections lead to $Mo_6X^i_8X^a_{4/2}X^a_2$ layers that are interpenetrated and held together through van der Waals contacts between halogen ligands of adjacent layers.[4] In the early 1960s, Sheldon reported the possibility of ligand exchanges within the unit without destruction of the Mo_6 cluster. In particular, Mo_6Cl_{12} can be converted in Mo_6 bromides and iodides in fused lithium bromide or iodide.[5] Moreover, he showed that it is rapidly disproportionated in fused KCl (m.p. 770 °C) to molybdenum metal and $K_3[Mo^{III}Cl_6]$ based on discrete $[Mo^{III}Cl_6]^{3-}$ ions. For a stoichiometric KCl/Mo_6Cl_{12} (i.e. 2:1) ratio, an excision reaction occurs instead of disproportionation leading to the pure chloride $K_2[Mo_6Cl_{14}]$ in which the $[Mo_6Cl_{14}]^{2-}$ units are discrete.[6] Mo_6Br_{12} exhibits a similar behaviour with bromide alkali salts[7] but hitherto no crystal structure has been reported with discrete $[Mo^{III}Br_6]^{3-}$ ions. On the other hand, the solid-state reaction of Mo_6X_{12} halides with chalcogens at high temperature enables the substitution of chalcogen for halogen.[8]

In this work, we evidence that the reaction between Mo_6Br_{12} and RbBr in the presence of Se or Te leads to a partial disproportionation of Mo_6Br_{12} into Mo and $[Mo^{III}Br_6]^{3-}$ as well as the substitution of one chalcogen for one bromine in an inner position to form the double-salts $Rb_3[Mo_6Br^i_7Y^iBr^a_6](Rb_3[MoBr_6])_3$ (Y = Te, Se) (**1**, $Rb_{12}Mo_9Br_{31}Te$ and **2**, $Rb_{12}Mo_9Br_{31}Se$). These compounds

[a] K. Kirakci, Dr. S. Cordier, Dr. C. Perrin
Laboratoire de Chimie du Solide et Inorganique Moléculaire
UMR 6226 CNRS Sciences Chimiques de Rennes
Université de Rennes 1
Avenue du Général Leclerc, 35042 Rennes Cedex (France)
Fax: (+33) 2-23-23-67-99
E-mail: Stephane.cordier@univ-rennes1.fr

are built up from $[Mo^{III}Br_6]^{3-}$ ions and $[Mo_6Br^i_7Y^iBr^a_6]^{3-}$ cluster units characterised by a random distribution of seven bromine and one chalcogen atoms on the eight inner positions. Such a distribution implies a static orientational disorder of the $[Mo_6Br^i_7Y^iBr^a_6]^{3-}$ units around the origin of the unit cell. The number of valence electrons per Mo_6 is found to be 24, corresponding to Mo^{II}, whilst the oxidation state of Mo in the $[Mo^{III}Br_6]^{3-}$ complexes is +3. Magnetic measurements have confirmed the oxidation states of molybdenum in this salt. It is worth noting that the Br^a–Br^a interunit distance is only 3.252 Å, which is much lower than the sum of van der Waals radii (3.70 Å).[9] The solid-state reactivity of Mo_6Br_{12} will be analysed and the structural findings will be discussed and compared with those of related compounds based on similar cluster units or complexes.

Results and discussion

Description of the structures of $Rb_{12}Mo_9Br_{31}Te$ (1) and $Rb_{12}Mo_9Br_{31}Se$ (2): Relevant interatomic distances for **1** and **2** are reported in Tables 1 and 2 respectively. Salt **1** crystallises in the cubic system (space group $Pm\bar{3}m$, No. 221). The structure is based on $[MoBr_6]^{3-}$ octahedral complexes (Figure 1) and $[Mo_6Br^i_7Te^iBr^a_6]^{3-}$ discrete anionic units (Figure 2) in which the Mo_6 cluster is face-capped by eight inner ligands. The average unit is characterised by a random distribution of one tellurium and seven bromine atoms on the eight inner positions. Such a distribution implies that the $[Mo_6Br^i_7Te^iBr^a_6]^{3-}$ units are statically and orientationally disordered. The presence of Te on the inner position induces a local C_3 symmetry. Indeed, the apparent O_h symmetry of the $[Mo_6Br^i_7Te^iBr^a_6]$ units in the $Pm\bar{3}m$ space group results from the static orientational disorder around the origin of the unit cell. Similar features have been encountered and discussed for Nb_6 cluster compounds based on $Nb_6L^i_{12}L^a_6$ units.[10] The centres of cluster units occupy the apices of the cubic unit cell (Figure 3). Mo and Br^a are located on the

Table 1. Selected interatomic distances [Å] in **1**.

$Mo_6Br_{13}Te$ unit		
Mo1–Mo2	2.6341(9)	×12
Mo1–Br1	2.589(1)	×6
Mo1–Br2	2.608(3)	×8
Mo1–Te2	2.73(2)	×8
$MoBr_6$ complex		
Mo2–Br3	2.606(1)	×2
Mo2–Br4	2.6026(7)	×4
rubidium environment		
Rb1–Br4	3.5274(1)	×4
Rb1–Br1	3.6564(9)	×2
Rb1–Br3	3.7733(7)	×2
Rb1–Br2	4.286(2)	×2
Rb1–Te2	4.18(2)	×2
Rb2–Br3	3.472(1)	×6
Br–Br contacts		
Br1–Br1	3.252(1)	×6
Br2–Br4	3.854(2)	×4

Table 2. Selected interatomic distances [Å] in **2**.

$Mo_6Br_{13}Se$ unit		
Mo1–Mo2	2.626(1)	×12
Mo1–Br1	2.590(2)	×6
Mo1 L2	2.597(1)	×8
$MoBr_6$ complex		
Mo2–Br3	2.599(2)	×2
Mo2–Br4	2.599(1)	×4
rubidium environment		
Rb1–Br4	3.5222(9)	×4
Rb1–Br1	3.631(2)	×2
Rb1–Br3	3.788(1)	×2
Rb1 L2	4.286(1)	×2
Rb2–Br3	3.473(2)	×6
Br–Br contacts		
Br1–Br1	3.251(2)	×6
Br2–Br4	3.857(1)	×4

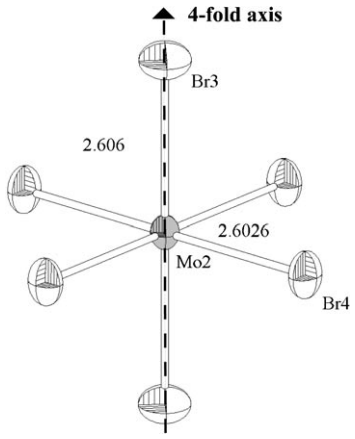

Figure 1. Representation of the octahedral $MoBr_6$ complex. Displacement ellipsoids are shown at the 50% probability level.

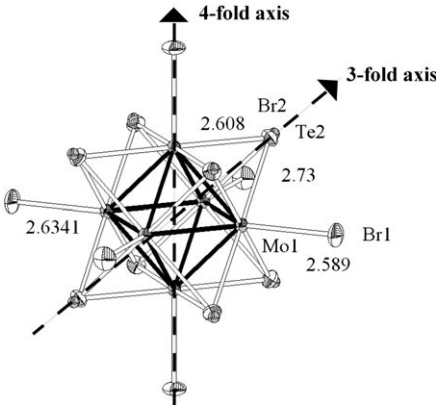

Figure 2. Representation of the $Mo_6Br_{13}Te$ unit. Displacement ellipsoids are shown at the 50% probability level. Locally only one of the two represented positions Te1 and Br1 is occupied.

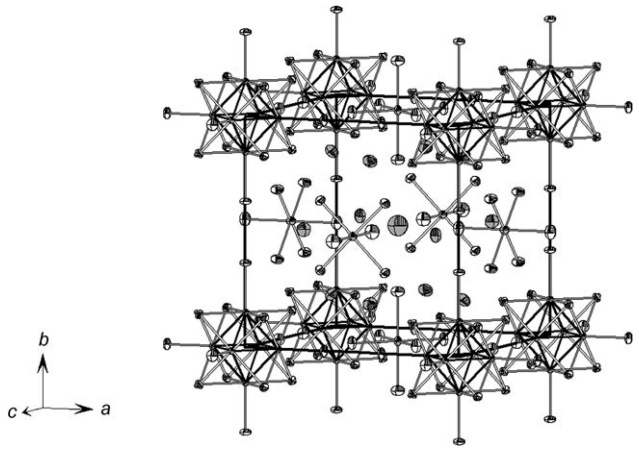

Figure 3. Representation of the $Rb_3[Mo_6Br_{13}Te](Rb_3[MoBr_6])_3$ unit cell (represented in bold). Displacement ellipsoids are shown at the 50% probability level.

edge of the units along one fourfold axis. The Mo atom of the $[MoBr_6]^{3-}$ entity lies at the centre of the faces, with the Mo–Br3 direction perpendicular to the faces and it merges with another fourfold axis. The $[MoBr_6]^{3-}$ complexes describe a large $([MoBr_6]^{3-})_6$ octahedron. Twelve distorted sites, each based on two $[Mo_6Br^i{}_7Te^iBr^a{}_6]^{3-}$ units and two $[MoBr_6]^{3-}$ entities, are generated at a 12*j* Wyckoff position (Figure 4, top) and are statistically occupied by Rb1 (98.4(3)%). It merges with the centroid of the distorted tetrahedron formed by two units belonging to one edge of the unit cell and by two $[MoBr_6]^{3-}$ entities belonging to one edge the $([MoBr_6]^{3-})_6$ octahedron. Each of the two $[MoBr_6]^{3-}$ complexes brings two Br4 and one Br3 atoms to complete the Rb1 coordination site (Rb1–Br4: 3.527 Å, Rb1–Br3: 3.773 Å). Two apical and two inner ligands from two cluster units complete this coordination site (Rb1–Br^a: 3.656 Å, Rb1–Br2: 4.286 Å, Rb1–Te2: 4.180 Å). Another cationic site located on the 1*b* Wyckoff position and statistically occupied by Rb2 (8(2)%) is generated at the centre of the unit cell corresponding also to the centre of the $([MoBr_6]^{3-})_6$ octahedron (Figure 4, bottom). The Rb2 atom lies in an octahedral site surrounded by bromine belonging to six $[MoBr_6]^{3-}$ complexes (Rb–Br 3.472(1) Å). The selenium homologue **2** is isostructural with **1**. The evolution of interatomic distances between **1** and **2** is related to the discrepancy between the ionic radii of Te and Se. One can note in particular a slight increase of Mo–Mo bond lengths, but no significant change in the distances of the $[MoBr_6]^{3-}$ complex as well as in the Br–Br contacts within the standard deviations.

Comparison between the structures of 1 ($Pm\bar{3}m$) and that of $Rb_{2.5}Mo_6Br_{13.5}Te_{0.5}$ ($Pn\bar{3}$): The common structural feature between the structures of **1** and $Rb_{2.5}Mo_6Br_{13.5}Te_{0.5}$[11] is that they are both based on $[Mo_6Br^i{}_7Te^iBr^a{}_6]^{3-}$ units. From the point of view of the stacking, the structure of **1** is related to that of $Rb_{2.5}Mo_6Br_{13.5}Te_{0.5}$ ($Pn\bar{3}$). In $Rb_{2.5}Mo_6Br_{13.5}Te_{0.5}$, the layers are stacked in an ABC sequence along the [111] direction. The projection of one unit layer of $Rb_{2.5}Mo_6Br_{13.5}Te_{0.5}$ is represented in Figure 5 (top). The same projection of a layer built from Mo_6 cluster units and $[MoBr_6]^{3-}$ complexes is represented in Figure 5 (bottom) for comparison. One can see that these projections are closely related. In $Rb_{2.5}Mo_6Br_{13.5}Te_{0.5}$, the unit oriented along the [111] direction is surrounded by six other units tilted by 45° versus the [111] direction corresponding to an orientation along the [1–11], [–1–11] and [–111] directions. In **1**, these tilted units are replaced by $[MoBr_6]^{3-}$ complexes. This change leads to new cationic sites. In $Rb_{2.5}Mo_6Br_{13.5}Te_{0.5}$, the octahedral unit cavities generated by the ABC stacking are fully occupied by rubidium cations. On the other hand, only $^3/_4$ of the tetrahedral cavities (centroid on a 6*d* Wyckoff position) are occupied, whilst the other $^1/_4$, located on the [111] axis (2*a* Wyckoff position), are empty owing to steric hindrance of inner ligands. In **1**, the $[Mo_6Br^i{}_7Te^iBr^a{}_6]^{3-}$ ionic units are located in a sphere with a diameter roughly equal to 8.90 Å and the $[MoBr_6]^{3-}$ complexes in a sphere with a diameter roughly equal to 5.21 Å. Despite this discrepancy of their diameter, the $[Mo_6Br^i{}_7Te^iBr^a{}_6]^{3-}$ and $[MoBr_6]^{3-}$ complexes are arranged according to a close-packing mode within the layer with Br4–Br2 contacts of 3.854 Å close to the value expected for van der Waals contacts. Regardless the type of anions, this packing generates octahedral and

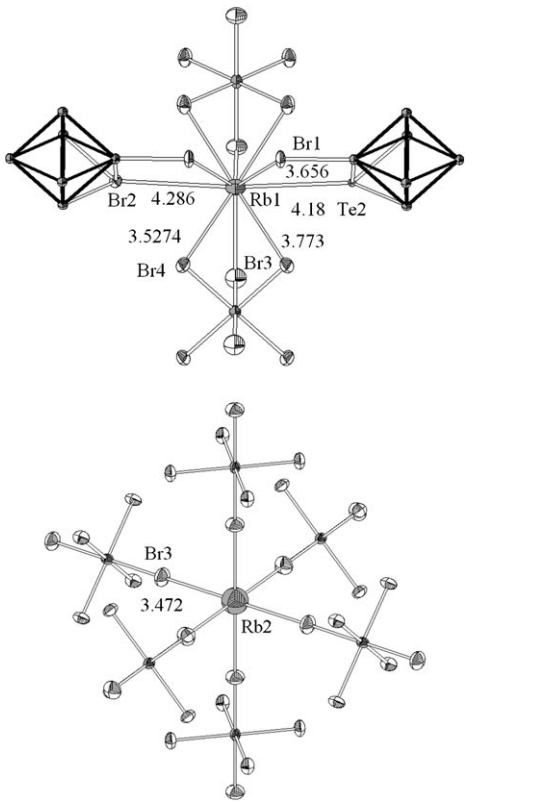

Figure 4. Top: Rb1 environment. Displacement ellipsoids are shown at the 50% probability level. For sake of clarity, only the ligands of the clusters belonging to the rubidium coordination sphere are represented. Bottom: Rb2 environment. Displacement ellipsoids are shown at the 50% probability level.

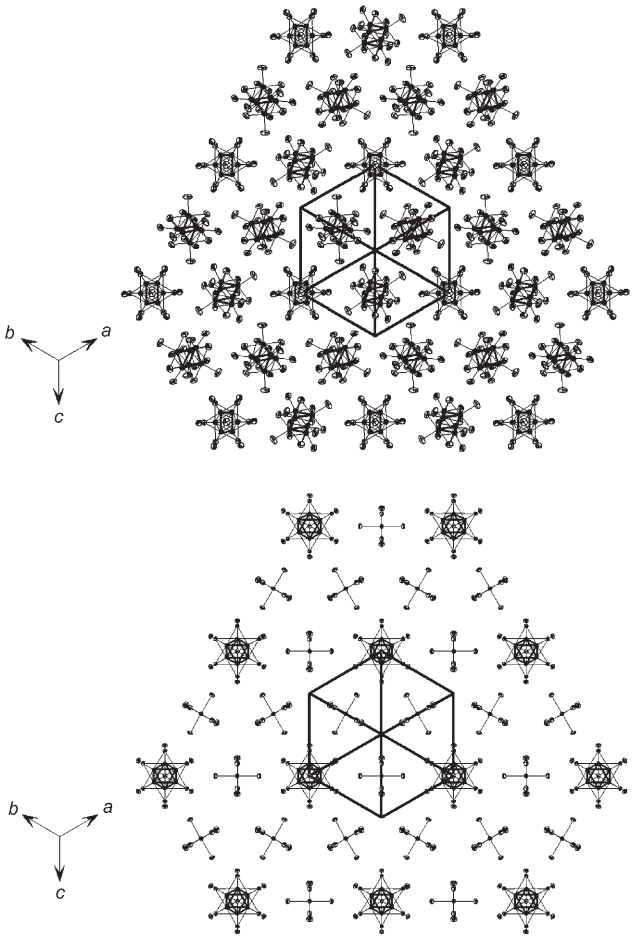

Figure 5. Top: Projection of an unit layer along [111] in $Rb_{2.5}Mo_6Br_{13.5}Te_{0.5}$. Bottom: Projection of an unit layer along [111] in $Rb_3[Mo_6Br_{13}Te](Rb_3[MoBr_6])_3$.

tetrahedral voids. Owing to the disposition of anions, the distance between the centroids of tetrahedral cavities and the L4 ligand is too short to be occupied by counterions (2.069 Å from Br4 and 1.916 Å from Te4). This resembles the steric hindrance of the ligand in $Rb_{2.5}Mo_6Br_{13.5}Te_{0.5}$ for the tetrahedral site located in the [111] direction. On the other hand, the distance between the middle of the edges of the unit cell and the Br^a ligands is found to be 1.626 Å, preventing the occupation of octahedral cavities centred on this position. The other octahedral cavity formed by the anions located at the centre of the unit cell is occupied by Rb2 (Figure 4 bottom).

Discrete $[Mo^{III}Br_6]^{3-}$ complexes in the solid state: Although isolated $[MoBr_6]^{3-}$ complexes have been characterised in highly concentrated solutions starting from $[MoBr_3(NH_3)_3]^{3-}$ complexes,[12] salts **1** and **2** constitute the first examples of solid-state compounds containing the discrete $[MoBr_6]^{3-}$ complex. Indeed, hitherto, no compound based on discrete triple-charged $[MoBr_6]^{3-}$ ions have been reported, although some compounds with double-charged ions have been isolated, for instance $[PPh_3Me]_2[MoBr_6]$ (average interatomic Mo–Br distance is 2.532 Å).[13] However, some complexes built up from Mo^{III}, Br^- and neutral donor ligands have been reported, for example, $(NH_4)_2[MoBr_5(H_2O)]$ or TPP-$[MoBr_4(Py)_2]$ (TPP = tetraphenylphosphonium).[14] The TPP-$[MoBr_4(Py)_2]$ complex is based on a $[Mo^{III}Br_4(Py)_2]^-$ monocharged complex with Mo–Br bond lengths ranging from 2.5761(7)–2.5831(7) Å with an average value of 2.580 Å. $(NH_4)_2[MoBr_5(H_2O)]$ is based on double-charged $[Mo^{III}Br_5(H_2O)]^{2-}$ complex with Mo–Br bond lengths that vary within the range 2.560(2) Å-2.583(1) Å with an average value of 2.580 Å. These average values of the Mo–Br bond lengths are smaller than those observed in **1** (2.606 Å) and **2** (2.599 Å).

Comparison with related compounds based on M_6 clusters and MX_6 complexes: Although based on edge-bridged $M_6L^i_{12}L^a_6$ units, instead of $M_6L^i_8L^a_6$ as in compounds **1** and **2**, two related examples of mixed oxidation compounds containing M_6 clusters and discrete M cations at a higher oxidation state have been reported: Zr_6Cl_{12}–M_2ZrCl_6 (M = Na, K, Cs)[15] and the Na_2NbF_6–$Nb_6L^i_{12-x}F^i_xF^{a-a}_{6/2}$ series ($x = 4$ for Cl and $x = 8$ for Br).[16] Zr_6Cl_{12}–M_2ZrCl_6 was obtained by decomposition of ZrClH in the presence of the corresponding chloride salt. In the zirconium compound, the $[Zr_6Cl^i_{12}L^a_6]$ units share their apical chlorine ligands with those of $[ZrCl_6]$ complexes. This compound can then better be written as $M_2ZrZr_6Cl_{18}$ in which the M and Zr^{4+} cations are located in the tetrahedral and octahedral cavities generated by an ABC close packing of the units. The Na_2NbF_6–$Nb_6L^i_{12-x}F^i_xF^{a-a}_{6/2}$ series was obtained by reduction of NbF_5 and NbX_5 by niobium metal in the presence of NaX. These series are based on $[M_6L^i_{12}F^a_6]^-$ units and $[MF_6]^-$ complexes. They crystallise in the $Pm\bar{3}m$ space group and exhibit a structure similar to those of **1** and **2**. The units are located on the apices of the cubic unit cell, but share apical ligands to form a $M_6L^i_{12}F^{a-a}_{6/2}$ three-dimensional framework. The $[NbF_6]$ complexes are located at the centre of the unit cell and the sodium atoms statically occupy positions close to the centre of the unit cell.

Br–Br contacts: The Br^a–Br^a distance between the units is very short (3.252 Å) and is much lower than the sum of the van der Waals radii (3.70 Å). This value can, however, be compared with those reported in reference [17]. For example, the Br–Br ionic–ionic contacts between the PBr_4^+ and Br^- ions in PBr_5 or between the PBr_4^+ and Br_3^- ions in PBr_7.[18] Note that this value is very close to the intermolecular contacts between dibromine molecules in solid Br_2 (3.30 Å).[19] In $[PPh_4][I_3Br_4]$,[20] the $[I_3Br_4]^-$ ions are dimerised through a Br–Br contact with a length of 3.367(3) Å. It turns out that only the related compound $La_{48}Br_{81}Os_8$,[21] based on La_6 clusters centred by Os, is also characterised by similar unusual short Br–Br contacts. In $La_{48}Br_{81}Os_8$, the La_6(Os) clusters are heavily interbridged by Br atoms found both in face-capping and edge-bridging positions. They exhibit in average 19.63 bonded Br atoms per La_6Os cluster to be compared to the usual 18 for $La_6Br^i_{12}Br^a_6$(Os) cluster

units. This astonishing bromide contains unusual Br^{i-a-a} functions and each lanthanum atom can be bound to more than one Br^a ligand. The strong structural constraints result in particular in a cell volume 10% less than for an equivalent hypothetical $La_6Br_{10}Os$ and short Br–Br contacts. The smallest ones are in the range 3.300(6)–3.393(6) Å.

The short Br^a–Br^a contacts in **1** and **2** must be related to the coexistence of two anionic species within the structure with different spherical diameters ($[Mo_6Br^i_7Y^iBr^a_6]^{3-}$: ≈8.90 Å; $[MoBr_6]^{3-}$: ≈5.21 Å). The structure of these double salts can be considered as a $Rb_3[Mo_6Br^i_7Y^iBr^a_6]$ salt embedded in a $Rb_3[MoBr_6]$ matrix according to a 1/3 ratio. The units are arranged in such a way that each Mo–Br^a bond from a unit that merges with the edge of the unit cell is oriented towards a Br^a–Mo bond from another unit. The coulombic interactions between anions and cations involve a compression of the units along the edges of the unit cell, resulting in a compression of the Mo–Br^a bond and short Br^a–Br^a contacts. This assumption is also supported by the short Mo–Br^a bond length (2.589(1)) Å compared to related Mo_6 cluster units.[11]

Chemistry of molybdenum bromides and concluding remarks: The reaction between Mo_6Br_{12} and a stoichiometric amount of an alkali salt leads to the formation of the $A_xMo_6Br_{14}$ series based on discrete $[Mo_6Br^i_8Br^a_6]^{2-}$ units. The charge of the unit can be increased by the substitution of chalcogen for halogen atoms. Indeed, monosubstituted units have been obtained in $Rb_{2+x}Mo_6Br^i_{8-x}Y^i_xBr^a_6$[11] while disubstituted units have been obtained in the $Cs_4Mo_6Br_{12}Y_2$ (Y = S, Se) series.[22] Let us recall that the $Rb_{2+x}Mo_6Br^i_{8-x}Y^i_xBr^a_6$ series ($x = 0.5$ for Y = Te ; $0.25 \le x \le 0.7$ for Y = Se) are built up from $[Mo_6Br^i_{8-x}Y^i_xBr^a_6]^{(2+x)-}$ average anionic units—corresponding to a mixture of $(1-x)$-$[Mo_6Br_{14}]^{2-}$ with $x[Mo_6Br_{13}Y]^{3-}$—associated with $(2+x)$ Rb^+ counterions. In the present new series, no range of homogeneity has been observed meaning that only the $[Mo_6Br_{13}Y]^{3-}$ species is present within the solid. From a chemical point of view, it transpires that the reaction between Mo_6Br_{12} and an excess of alkali salt leads to a disproportionation of Mo_6Br_{12} into Mo and $[Mo^{III}Br_6]^{3-}$ ($3ABr + 3Mo^{II}Br_2 \rightarrow Mo + A_3Mo_2{}^{III}Br_9$). Consequently, the increase in the RbBr/$Mo_6{}^{II}Br_{12}$ ratio in the loaded composition leads to final product poorer in $Rb_2Mo_6Br_{14}$ and richer in Mo and $A_3Mo_2{}^{III}Br_9$. The presence of chalcogens in the loaded composition favours the formation of the $[Mo_6Br^i_7Y^iBr^a_6]^{3-}$ anionic cluster unit. This enables the formation of hybrid solid-state compounds containing both $[Mo^{III}Br_6]^{3-}$ ions and $[Mo_6Br^i_7Y^iBr^a_6]^{3-}$ ionic cluster units. Further experiments showed that higher reaction yields for **1** and **2** are obtained starting from RbBr, $MoBr_3$, Mo_6Br_{12}, Mo and Y for stoichiometrically loaded compositions.

Experimental Section

Synthesis of $Rb_{12}Mo_9Br_{31}Te$ and $Rb_{12}Mo_9Br_{31}Se$: Mo_6Br_{12} was obtained by decomposition of $MoBr_3$—prepared by reaction of molybdenum powder in Br_2 flow at 680 °C—under a N_2 flow at the same temperature.[4] Single-crystals of $Rb_{12}Mo_9Br_{31}Se$ and $Rb_{12}Mo_9Br_{31}Te$ were initially obtained from reactions as secondary phases in reactions designed to synthesise the $Rb_{2+x}Mo_6Br^i_{8-x}Y_xBr^a_6$ chalcogenobromides. After a preliminary structural determination, the title series was obtained from a powdered mixture (0.5 g) of RbBr, Mo_6Br_{12} and Y (Y = Te, Se) with the ratios 12:(19/2):1. The equation of the reaction can be therefore written: $12\,RbBr + 19/12\,Mo_6Br_{12} + Y \rightarrow Rb_{12}[MoBr_6]_3[Mo_6Br^i_7Y^iBr^a_6] + {}^1/_2\,Mo$. Powders were ground, pelleted and placed into a silica tube. Once sealed under vacuum, the tube was heated for three days at 900 °C. The analysis of the X-ray powder patterns evidenced the presence of Mo, $Rb_2Mo_6Br_{14}$ and $Rb_{2.5}Mo_6Br_{13.5}Y_{0.5}$ as secondary phases along with $Rb_{12}[MoBr_6]_3[Mo_6Br^i_7Te^iBr^a_6]$ as the major product. It must be pointed out that when RbBr contains traces of moisture, a partial substitution of O for Br was observed in the $[MoBr_6]$ complex, leading to a reduction of the anionic charge and consequently of the rubidium content in the title compound.

Chemical analysis: Elemental content was determined by chemical analyses of single crystals at the Centre for Scanning Electron Microscopy and Microanalyses of Rennes 1 University (France) by energy dispersive spectrometry (EDS) using a scanning electron microscope JEOL JSM 6400 equipped with a microprobe EDS OXFORD LINK ISIS. The atomic percentages obtained for several single crystals for **2** and **1** were Rb 25, Mo 19, Br 54, Se 2 and Rb 24, Mo 18, Br 56, Te 2, respectively; elemental analysis calcd (%) for $Rb_{12}Mo_9Br_{31}Y$: Rb 22.64, Mo 16.98, Br 58.49, Y 1.89.

Magnetic measurements: Magnetic susceptibility measurements were performed with a SQUID susceptometer on 30 mg of selected $Rb_{12}Mo_9Br_{31}Se$ single crystals within the temperature range 2–300 K at 500 G. The magnetic data, in the form of $1/\chi$ versus T are shown in Figure 6. The susceptibility follows a Curie law with an experimental

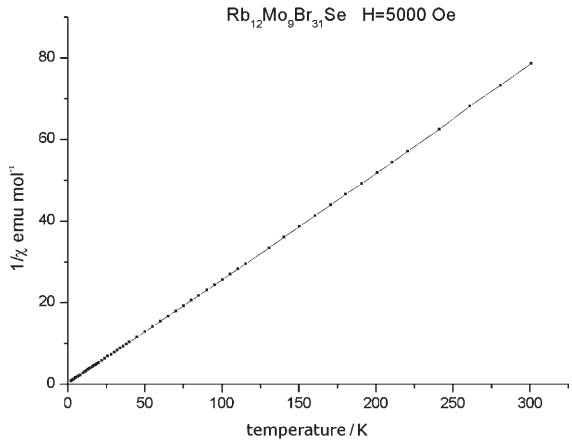

Figure 6. Representation of the inverse magnetic susceptibility versus T for **1**.

$\mu_{eff} = 3.95\ \mu_B$ and is consistent with the presence of Mo^{III} in the $[MoBr_6]^{3-}$ complex and a VEC value of 24 for the $[Mo_6Br^i_7Te^iBr^a_6]^{3-}$ unit. Indeed, the theoretical magnetic moment per Mo^{III} at 300 K is $\mu_{th} = 3.87\ \mu_B$ is consistent with a $S = 3/2$ ground state and a VEC value of 24 corresponds to a nonmagnetic cluster.

Crystal structure analysis: Single-crystal X-ray diffraction data of $Rb_{12}Mo_9Br_{31}Te$ and $Rb_{12}Mo_9Br_{31}Se$ were collected at room temperature on a Nonius KappaCCD area-detector X-ray diffractometer with $Mo_{K\alpha}$

radiation ($\lambda = 0.71073$ Å) (Centre de Diffractométrie de l'Université de Rennes 1, France). Details of data collections and structure refinements are reported in Table 3. Positional and equivalent atomic displacement parameters are reported in Tables 4 and 5 for **1** and **2**, respectively. The data processing was performed by the EvalCCD analysis software[23] and absorption corrections were applied through the SADABS program.[24] Among the possible space groups deduced from the observed systematic extinctions, the refinement procedure enabled to retain unambiguously the $Pm\bar{3}m$ centrosymmetric space group for the two title compounds. The structures were solved by direct methods by using the SIR97 program.[25] Subsequent structural refinements by least-squares techniques, combined with difference Fourier syntheses, were performed using SHELXL-97.[26] The structure of $Rb_{12}Mo_9Br_{31}Te$ is based on a $[Mo_6Br^i{}_7Te^iBr^a{}_6]$ average unit and on a $[MoBr_6]$ complex of O_h and D_{4h} symmetry, respectively. The $[MoBr_6]$ complex is built up from Mo1, Br3 and Br4 located on the 3*c*, 6*f* and 12*i* Wyckoff positions, respectively. The $[Mo_6Br^i{}_7Te^iBr^a{}_6]$ unit is built up from Mo2 and apical bromine Br1 located both on 6*e* Wyckoff positions. During the refinement procedure, it was firstly assumed that the inner Br2 fully occupied an 8*g* position, but after several cycles of refinements, it turned out that an electronic peak remained close to Br2 at a distance from molybdenum corresponding to a Mo–Te bond length. Tellurium Te2 was then introduced on this residue with the same atomic displacement parameter as Br2. The sum of the occupancies of Br2 and Te2 was restricted to the value corresponding to a fully occupied 8*g* position. Afterwards, the first two restraints were progressively relaxed during the convergence, leading to final positions in agreement with reliable Mo–(Br, Te) interatomic distances. Owing to the small occupancy of tellurium, this atom was refined isotropically. Rb1 and Rb2 statistically occupy a 12*j* and a 1*b* Wyckoff position. The final formula deduced from the structural refinement is $Rb_{11.90(4)}Mo_9Br_{31.34(6)}Te_{0.66(6)}$. This formula was rounded to $Rb_{12}Mo_9Br_{31}Te$ considering that the number of valence electrons is constant and equal to 24. Indeed, a Te content lower than 1 would imply a VEC value higher than 24 and the electronic occupancy of Mo–Mo antibonding levels.

The structure of $Rb_{12}Mo_9Br_{31}Se$ is isostructural with that of $Rb_{12}Mo_9Br_{31}Te$. Although X-ray diffraction techniques are not appropriate to discriminate Se and Br owing to their close scattering factors, these two elements were assumed randomly distributed on the inner ligand position (L2) for $Rb_{12}Mo_9Br_{31}Se$ as found experimentally for the tellurium compound. The presence of selenium in the compound was confirmed by EDS analysis performed on several selected crystals. The final formula deduced from structural determination was $Rb_{11.83(6)}Mo_9Br_{31}Se$ and was rounded to $Rb_{12}Mo_9Br_{31}Se$. For both compounds the refined rubidium content is 12 within the standard deviations. As stressed above for $Rb_{12}Mo_9Br_{31}Te$, the VEC value of 24 implies the presence of exactly one chalcogen per unit for corresponding Rb content equal to 12.

Further details on the crystal structure investigation(s) may be obtained from the Fachinformationszentrum Karlsruhe, 76344 Eggenstein-Leopoldshafen, Germany (fax: (+49) 7247-808-666; e-mail: crysdata@fiz-karlsruhe.de), on quoting the depository numbers CSD-416123 (**1**) and CSD-416124 (**2**).

Table 3. Crystal data for the structure determinations of **1** and **2**.

	1	**2**
formula	$Rb_{11.90(4)}Mo_9Br_{31.34(6)}Te_{0.66(6)}$	$Rb_{11.83(6)}Mo_9Br_{31}Se$
M_r	4493.91	4446.22
space group	$Pm\bar{3}m$	$Pm\bar{3}m$
a [Å]	12.1558(2)	12.144(3)
V [Å^3]	1796.18(5)	1791.0(8)
Z	1	1
ρ_{calcd} [g cm^{-3}]	4.155	4.122
crystal dimensions [mm^3]	$0.052 \times 0.085 \times 0.128$	$0.038 \times 0.049 \times 0.056$
reflns collected	22700	23108
unique reflns	692	466
R_{int} (all data)	0.0826	0.103
μ [mm^{-1}]	27.244	27.483
T [°C]	20	20
obsvd refls [$I > 2\sigma(I)$]	529	409
parameters	30	27
R_1[a] [$I > 2\sigma(I)$]	0.028	0.028
wR_2[a] (all data)	0.050	0.057
$\Delta\rho_{min}/\Delta\rho_{max}$ [e Å^{-3}]	−0.857/1.519	−0.588/0.876

[a] $R_1 = \Sigma_{hkl}||F_o| - |F_c||/\Sigma_{hkl}|F_o|$; $wR_2 = [\Sigma_{hkl}[w(F_o^2 - F_c^2)^2]/\Sigma_{hkl}[w(F_o^2)^2]]^{1/2}$.

Table 4. Positional and displacement parameters [Å^2] for **1**.

atom	position	x	y	z	occupancy	U_{eq}
Mo1	6*e*	0.84677(5)	0	0	1	0.0121(1)
Mo2	3*c*	1/2	0	1/2	1	0.0212(2)
Br1	6*e*	0.63377(7)	0	0	1	0.0300(2)
Br2	8*g*	0.8482(2)	−0.1517(2)	0.8482(2)	0.918(7)	0.0199(7)
Te2	8*g*	0.841(1)	−0.159(1)	0.841(1)	0.082(7)	0.008(3)
Br3	6*f*	1/2	0.21438(9)	1/2	1	0.0492(3)
Br4	12*i*	0.65140(4)	0	0.65140(4)	1	0.0335(2)
Rb1	12*j*	0.80949(6)	−0.19051(6)	1/2	0.984(3)	0.0486(3)
Rb2	1*b*	1/2	1/2	1/2	0.08(2)	0.12(3)

Table 5. Positional and displacement parameters [Å^2] for **2**.

atom	position	x	y	z	occupancy	U_{eq}
Mo1	6*e*	0.84710(8)	0	0	1	0.0140(2)
Mo2	3*c*	1/2	0	1/2	1	0.0227(4)
Br1	6*e*	0.6338(1)	0	0	1	0.0308(3)
L2[a]	8*g*	0.84881(5)	−0.15119(5)	0.84881(5)	1	0.0212(3)
Br3	6*f*	1/2	0.2139(1)	1/2	1	0.0531(5)
Br4	12*i*	0.65132(6)	0	0.65132(6)	1	0.0353(3)
Rb1	12*j*	0.81095(8)	−0.18905(8)	1/2	0.982(5)	0.0523(5)
Rb2	1*b*	1/2	1/2	1/2	0.045(2)	0.06(5)

[a] L2 = (7/8 Br + 1/8 Se).

Acknowledgements

The "Centre de Diffractométrie de l'Université de Rennes 1" is acknowledged for the data collection on the Nonius KappaCCD X-ray diffractometer. In particular, we thank Dr. T. Roisnel for the useful advice. We are also indebted to the "Fondation Langlois" for its financial support. K.K. is grateful for Ph.D. grant from the "Ministère de la Recherche".

[1] C. Brosset, *Ark. Kemi Mineral. Geol.* **1945**, 20A, No 7.
[2] C. W. Blomstrandt, *J. Prakt. Chem.* **1857**, *71*, 449.
[3] H. Schäfer, H. G. von Schnering, *Angew. Chem.* **1964**, *76*, 833.
[4] H. Schäfer, H. G. von Schnering, J. Tillack, F. Kuhnen, H. Wöhrle, H. Baumann, *Z. Anorg. Allg. Chem.* **1967**, *353*, 281.

[5] J. C. Sheldon, *J. Chem. Soc.* **1962**, 410.
[6] M. Potel, C. Perrin, A. Perrin, M. Sergent, *Mater. Res. Bull.* **1986**, *21*, 1239.
[7] K. Kirakci, S. Cordier, C. Perrin, *Z. Anorg. Allg. Chem.* **2005**, *631*, 411.
[8] a) C. Perrin, M. Potel, M. Sergent, *Acta Crystallogr. Sect. C* **1983**, *39*, 415; b) C. Perrin, M. Potel, M. Sergent, Ø. Fisher, *Mater. Res. Bull.* **1979**, *14*, 1505; c) C. Perrin, M. Sergent, F. Le Traon, A. Le Traon, *J. Solid State Chem.* **1978**, *25*, 197; d) C. Perrin, M. Sergent, *J. Chem. Res. Synop.* **1983**, *2*, 38.
[9] a) A. Bondi, *J. Phys. Chem.* **1964**, *68*, 441; b) R. S. Scott, R. Taylor, *J. Phys. Chem.* **1996**, *100*, 7384–7931.
[10] N. G. Naumov, S. Cordier, C. Perrin, *Solid State Sci.* **2005**, *12*, 1517.
[11] K. Kirakci, S. Cordier, O. Hernandez, T. Roisnel, F. Paul, C. Perrin, *J. Solid State Chem.* **2005**, *178*, 3117.
[12] M. Brorson, C. J. H. Jacobsen, I. Schmidt, J. Villadsen. *Inorg. Chim. Acta.* **1996**, *247* 189.
[13] I. Schmidt, U. Patt-Siebel, U. Müller, K. Dehnicke, *Z. Anorg. Allg. Chem.* **1988**, *556*, 57.
[14] J. V. Brenčič, B. Modec, *Acta Crystallogr. Sect. C* **1995**, *51*, 197–198.
[15] H. Imoto, J. D. Corbett, A. Cisar, *Inorg. Chem.* **1981**, *20*, 145.
[16] a) S. Cordier, A. Simon, *Solid State Sci.* **1999**, *1*, 199; b) S. Cordier, O. Hernandez, C. Perrin, *J. Fluorine Chem.* **2001**, *107*, 205.
[17] S. L. Lawton, D. M. Moh, R. C. Johnson, A. S. Knisely, *Inorg. Chem.* **1973**, *12*, 277.
[18] L. Breneman, R. D. Willet, *Acta Crystallogr.* **1967**, *23*, 467.
[19] H. T. Kalf, C. Romers, *Recl. Trav. Chim. Pays-Bas* **1966**, *85*, 198.
[20] R. Minkwitz, M. Berkei, R. Ludwig, *Inorg. Chem.* **2001**, *40*, 25.
[21] S. T. Hong, L. H. Hoistad, J. D. Corbett, *Inorg. Chem.* **2000**, *39*, 98.
[22] S. Cordier, N. Naumov, D. Salloum, F. Paul, C. Perrin, *Inorg. Chem.* **2004**, *43*, 219.
[23] A. J. M. Duisenberg, L. M. J. Kroon-Batenburg, A. M. M. Schreurs, *J. Appl. Crystallogr.* **2003**, *36*, 220.
[24] G. M. Sheldrick, SADABS version 2.03.Bruker AXS Inc., Madison,-Wisconsin, USA, **2002**.
[25] "A New Tool for Crystal Structure Determination and Refinement": A. Altomare, M. C. Burla, M. Camalli, G. Cascarano, C. Giacovazzo, A. Guagliardi, A. G. G. Moliterni, G. Polidori, R. Spagna, *J. Appl. Crystallogr.* **1999**, *32*, 115.
[26] G. M. Sheldrick, SHELXL-97: Program for the Refinement of Crystal Structures, University of Göttingen, Göttingen (Germany), **1997**.

Received: January 23, 2006
Published online: May 26, 2006

